CMST 7(1) 91-112 (2001) DOI:10.12921/cmst.2001.07.01.91-112

COMPUTATIONAL METHODS IN SCIENCE AND TECHNOLOGY 7 (1), 91-112 (2001)

THE STRUCTURE OF RAREFIED AND DENSIFIED $PbGeO_3$ AND $PbGeO_2$ GLASSES: A MOLECULAR DYNAMICS STUDY

JAROSŁAW RYBICKI[1,2], AGNIESZKA WITKOWSKA[1,2], GRZEGORZ BERGMAŃSKI[1], JAROSŁAW BOŚKO[1,2], GIORGIO MANCINI[3], SANDRO FELIZIANI[3]

[1] *Department of Solid State Physics, Faculty of Technical Physics and Applied Mathematics Technical University of Gdańsk, Narutowicza 11/12, 80-952 Gdańsk, Poland*

[2] *TASK Computer Centre, Narutowicza 11/12, 80-952 Gdańsk, Poland*

[3] *INFM UdR Camerino, Istituto di Matematica e Fisica, Universita di Camerino Madonna delle Carceri, Camerino (MC), Italy*

Abstract. The paper is dedicated to a molecular dynamics (MD) study of the structure of rarefied and densified lead-germanate glasses, of compositions $PbGeO_3$ and $PbGeO_2$. The simulations have been performed at constant volume for systems with densities of 3000, 4000, 5000, 6285 (normal density), 7000, and 8000 kg/m^3, using a two-body potential (Born-Mayer repulsive forces, and Coulomb forces due to full ionic charges). All the systems were initially prepared as well equilibrated hot melts, and then slowly cooled down to 300 K. The information on short-range correlations was obtained in a conventional way (from radial and angular distribution functions), while the middle-range order was studied via cation-anion ring analysis. In the paper, the short- and medium-range order in the rarefied and densified glasses is discussed and compared with the structure of the $PbGeO_3$ and $PbGeO_2$ glasses at normal conditions.

1. INTRODUCTION

Lead-silicate and lead-germanate glasses have been extensively investigated because of their numerous practical applications (e.g. [1, 2]). The best known are lead-silicate glasses, xPbO(1- x)Si0$_2$, $0.0 \le x \le 0.95$. They have high density, high thermal expansion coefficient, good transparency in the infrared range, and high refraction index (up to 2.15 at high PbO contents), and find wide industrial applications, e.g. in electronics and optoelectronics [2-4]. Lead-germanate glasses, xPbO(1 - x)GeO_2,$0.0 \le x \le 0.67$, are investigated to much lesser extent, and until now find fewer practical applications [5, 6].

It is well known that most glasses, depending on the preparation method, can have various densities at the same composition. In this respect, silica is probably the most studied material (e.g. [7-19]). Studies on low- and high-density forms of many binary silica glasses have also been performed. Recently, the research on densified germania has been undertaken [20], The structure of rarefied and densified germania glasses containing heavy-metal oxides, as far as the authors know, has not been studied until now, neither experimentally, nor theoretically.

The present contribution is dedicated to a molecular dynamics (MD) study of the structure of rarefied and densified lead-germanate glass of composition $PbGeO_3$, and its totally reduced counterpart, $PbGeO_2$. In order to see more clearly the structural feature characteristic for low- and high- density states we perform our simulations in a wide range of densities, from 3000 kg/m^3 to 8000 kg/m^3. Because no experimental data on the atomic-level structure of low- or high-density

states of the considered glasses are known, our MD results have a predictive character. However, the potential used in our simulations has been recently successfully applied for extensive MD study of the $xPbO(1 - x)GeO_2$ and $xPb(1 - x)GeO_2$ glasses in a wide range of stoichiometries at normal densities [21], giving a very good agreement with available experimental data. Thus we exploit the same potential for further MD studies believing that it reproduces well also the structure of rarefied and densified glasses.

The paper is organised as follows. In Section 2 we describe the applied simulation technique, and the data analysis methods. The simulation results are described and discussed in Sections 3, 4, and 5. In particular, Section 3 is dedicated to the isothermal compressibility coefficient of the $PbGeO_3$ and $PbGeO_2$ glasses. In Section 4 we describe in detail short-range order in unreduced, and reduced glasses. The medium-range order is described in Section 5. Section 6 contains conclusions.

2. SIMULATION TECHNIQUE

The molecular dynamics (MD) simulations have been performed in the constant volume regime (NVE ensemble). The atoms were assumed to interact by the two-body Born-Mayer-Huggins potential:

$$V_{ij}(r) = \frac{q_i q_j}{4\pi\varepsilon_0 r} + A_{ij}\exp\left(\left(\sigma_{ij} - r\right)/b_{ij}\right), \tag{1}$$

containing the Born-Mayer repulsive contribution, and Coulomb interactions. We used full ionic charges. The potential parameters A_{ij}, b_{ij} and σ_{ij} were taken from [21], where a good agreement between the structural experimental and MD data has been reported.

We simulated the $PbGeO_3$ and $PbGeO_2$ systems with constant densities of 3000, 4000, 5000, 6285, 7000, and 8000 kg/m^3. The numbers of atoms within the simulation box with usual periodic boundary conditions were equal to 2500 for unreduced glasses (500 Pb, 500 Ge, 1500 O atoms), and 2000 for reduced glasses (500 Pb, 500 Ge, 1000 O atoms). In dependence of density, the edge of the cubic simulation box varied from about 30 to about 45 Å. A large-scale simulation, with 20000 atoms within the simulation box, has been performed for reduced glass at normal density (i.e. 6285 kg/m^3). The pressures were calculated during the sampling runs from the virial theorem. The samples were initially prepared in a well equilibrated molten state at 10000 K, and slowly cooled down to 300 K, passing equilibrium states at 8000 K, 6000 K, 5000 K, 4000 K, 3000 K, 2500 K, 2000 K, 1500 K, 1000 K, and 600 K. The temperature scaling was applied whenever the rolling average of the temperature (calculated over last 100 time steps) went out from the interval $(T - \Delta T,\ T + \Delta T)$. At each intermediate temperature the system was being equilibrated during 30000 fs time steps, using $\Delta T = 100$ K for $T \geq 1000$ K, and $\Delta T = 20$ K and $\Delta T = 10$ K for $T = 600$ K and $T = 300$ K, respectively. Equilibrated systems were sampled during 10000 fs time steps. Such a run scheme corresponds to the average cooling rate of $2 \cdot 10^{13}$ K/s.

The resulting low- and normal-density (3000 kg/m^3 $\leq \rho \leq$ 6285 kg/m^3) structures turned out to be stable: the final 300 K-cofigurations have been relaxed at zero external pressure conditions,

and the volumes of the systems changed only by several percent (3-6%). Thus, the MD results obtained in this range of densities are supposed to refer to hypothetical "true" (equilibrium) low-density glasses. However, the densified structures we have obtained were not stable: instead of the volume relaxation we observed rather a continuous system expansion, with no tendency to any saturation. Thus, the high-density MD data ($\rho > 6285$ kg/m^3) are considered here rather as corresponding to the $PbGeO_3$ and $PbGeO_2$ glasses under positive hydrostatic pressure than to stable high-density phases.

The structural information on short-range correlations was obtained in a conventional way, mainly from radial and angular distribution functions (RDFs and ADFs, respectively). However, in order to describe the second, and further co-ordination shells, i.e. to describe the middle-range order, in addition to the RDFs and ADFs analysis one should use more advanced methods of the structure recognition. One of the possible approaches consists in the analysis of properly constructed clusters of edge and/or face sharing Voronoï polyhedra [22-24], This method, although veiy efficient in the detection of crystalline regions of various symmetry [25] works well for close packed systems. In open systems serious problems appear in the construction of the Voronoï network, and in the procedures eliminating short edges and small faces. In such cases, the cation-anion ring analysis seems to be an ideal tool for characterising the middle-range order. The middle-range order was studied mainly via cation-anion ring analysis, performed using a new highly efficient redundancy aware algorithm. The algorithm is based on the communication network simulation proposed for an efficient exact solution of the Ring Perception Problem [26], However, a new approach named "pre-filtering" technique [27, 28] has been recently developed to perceive rings in structures represented by 2-connected graphs. The structure of the determined basal rings was investigated using the ANELLI programme package [29, 30],

A series of tests on size-dependence of the results has been performed. The short range-order (RDFs, ADFs and distributions of co-ordination numbers) is the same as described below (for 2500- and 2000-atom samples) even in much smaller samples (with 500 and 400 atoms). However, the medium-range order (ring statistics) differs somewhat (especially in the long-ring part of the ring length distributions) in the $N = 2500$ (2000) and the $N = 500$ (400) atom samples. For this reason, a very time consuming 20000-atom simulation (mentioned above) has been performed. It turned out, that the ring length distributions are identical in the $N = 2000$, and the $N = 20000$ systems. Thus, the chosen system size, i.e. 2500 and 2000 atoms for unreduced and reduced glasses, respectively, is well above the minimum size necessary to obtain reasonable data on the short-range order, and simultaneously sufficient to get fully representative data on the medium-range order. We would like to add, that in the case of reduced glasses our $N = 2000$ atoms system is still too small to provide a size-independent statistic of metallic (lead) granules, and thus no data on the granule sizes and shapes are given in the present paper.

3. ISOTHERMAL COMPRESSIBILITY COEFFICIENT

The isothermal compressibility coefficient κ can be estimated as $d(\ln V)/dp$, where V is the volume of the simulation box, and p is the corresponding pressure. Figure 1 shows the *inF versus*

p relation. The slopes of the curves from the figure give the values of the κ coefficient (with minus sign). The κ coefficient estimated for unreduced glass in the pressure range from 0 to 6 GPa is close up to several percent to the experimental value, $\kappa = 3.2 - 10^{-5}$ MPa^{-1} [31],

As it is seen in Figure 1, the compressibility coefficient is a strongly non-linear function of pressure. For low-density structures, 3000 kg/m^3 $\leq \rho \leq$ 5000 kg/m^3, the calculated pressure is negative, so the glasses can be considered as expanded ones. Such expanded glasses have very high compression coefficients. Note, that the tenacity of thin threads ($\approx$ 10 μm of diameter) fabricated of $PbGeO_3$ glass amounts about 60 kg/mm^2 [32], so we can roughly assume, that at calculated internal pressures less than -1 GPa the system fragmentation can occur. Indeed, the shape of the (•) - curve in Figure 1 suggests a loss of the structure connectivity in this range of pressures (cf. Sections 5.2 and 5.3).

4. SHORT-RANGE ORDER

In this section we discuss the short-range ordering in the considered glasses, in particular the spatial distribution of the first neighbours of Ge atoms in unreduced, and totally reduced glasses (Sections 4.1, and 4.2, respectively), and the distribution of the first neighbours of Pb atoms (Section 4.3).

4. 1. GeO_2 subsystem - unreduced glasses

Figure 2 (panels A) shows the first peaks of radial distribution functions related to germanium cation and their first neighbours for three various densities. The corresponding angular distribution functions are shown in Figure 3, panels A. As it is seen in Figure 2, most of the first RDF peaks reveal rather significant asymmetry. As it has been shown in a number of papers, the RDFs in disordered systems can be decomposed in a short-range peak of a well-defined shape, and a long-range tail [33, 34], A simple Gaussian shape of the short-range peak of RDF is usually insufficient to describe accurately the short-range ordering in highly disordered systems. A useful parameterisation of the first RDF peak, as shown in [34, 35], has the form:

$$g(r) = \frac{Np(r)}{4\pi\rho r^2}, \tag{2}$$

where N is the co-ordination number, p is the density. The bond length probability density $p(r)$ is described by a Γ-like distribution. The corresponding formula, valid for $(r - R)\beta > -2\sigma$, reads:

$$p(r) = \frac{2}{\sigma \cdot |\beta| \cdot \Gamma(4/\beta^2)} \cdot \frac{4}{\beta^2} + \left(\frac{2 \cdot (r - R)}{\sigma \cdot \beta} \right)^{\frac{4}{\beta^2} - 1} \cdot \exp\left[- \left(\frac{2 \cdot (r - R)}{\sigma \cdot \beta} \right) \right]. \tag{3}$$

Here R is the average distance, σ^2 is the variance (Debye-Waller - like parameter), β is the asymmetry (skewness) parameter, and $\Gamma(x)$ is the Euler's gamma function, calculated for $x = 4/\beta^2$.

Inter-atomic distances

Table I contains the positions of the maxima, R_o of first Ge-0 and 0 - 0 RDFs' peaks, i.e. the most probable Ge-O and O-O distances, and the corresponding best-fit R, σ^2, β, and N values for

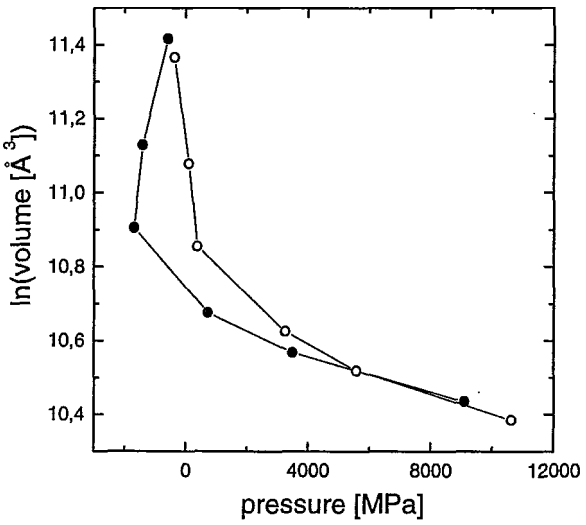

Fig. 1. Logarithm of the simulation box volume *versus* pressures calculated from the virial theorem for the $PbGeO_3$ (•) and PbGeO, (°) glasses. The subsequent points on each curve (from the right to the left) correspond to the densities of 8000 kg/m^3, 7000 kg/m^3, 6285 kg/m^3, 5000 kg/m^3, 4000 kg/m^3, and 3000 kg/m^3

unreduced glasses. The calculated most probable Ge-O distances, R_o, are almost density-independent (1.67-1.68 Å). The density behaviour of the mean Ge-O distance, R, is quite different. Its value in rarefied and normal-density glasses is equal to 1.68 Å, whereas in densified glasses, amounts to 1.69 Å and 1.72 Å for 7000 kg/m^3 and 8000 kg/m^3, respectively. The values of the Debye-Waller-like parameter, σ^2, and of the skewness parameter, β, are stable and very low for $\rho \leq 6285$ kg/m^3 (except for a remarkable increase of the Ge-O peak asymmetry at 6285 kg/m^3). The discrepancy between the values of the R_o and R parameters observed at higher densities is related to a significant increase of the peak skewness, β.

The most probable O-O distance, R_o, in rarefied glasses, is somewhat longer than at normal density (2.72 Å and 2.70 Å, respectively). In densified glasses the R_o values become significantly shorter. If the first O-O peak is approximated by a single Γ-like function (3), the mean distances, R, are less density dependent, and decrease only by 0.02 Å over the whole density range that was considered. The dispersion of the O-O distances is much wider than of the Ge-O distances: the σ^2 parameter is 3-4 times higher for the O-O correlation than for the Ge-O correlation. Also the skewness parameter, β, is rather high, and it increases with increasing density. The shortening of the mean O-O distance and increase of the σ^2 and β parameters with increasing density is accompanied by an increase of the average co-ordination number: from 4 for 3000 kg/m^3 to about 5.2 for 8000 kg/m^3. In densified structures, however, the first peak can be approximated much better using two superimposed Γ-like functions. The parameters of both peaks, denoted by (II) and (III), are given in Table I. Now the problem of the sub-peak's interpretation arises. This is not an easy task in this case, because both peaks are fairly close, and both are rather asymmetric. A detailed analysis suggests, that peak (III) (with $R \approx 2.76$ Å) is contributed mainly by the O-O distances in the faces of the GeO_4 tetrahedra. The less distant peak (II) (with $R \approx 2.59$ Å) is related predominantly to the oxygen atoms belonging to the first co-ordination shell of Pb^{2+} ions.

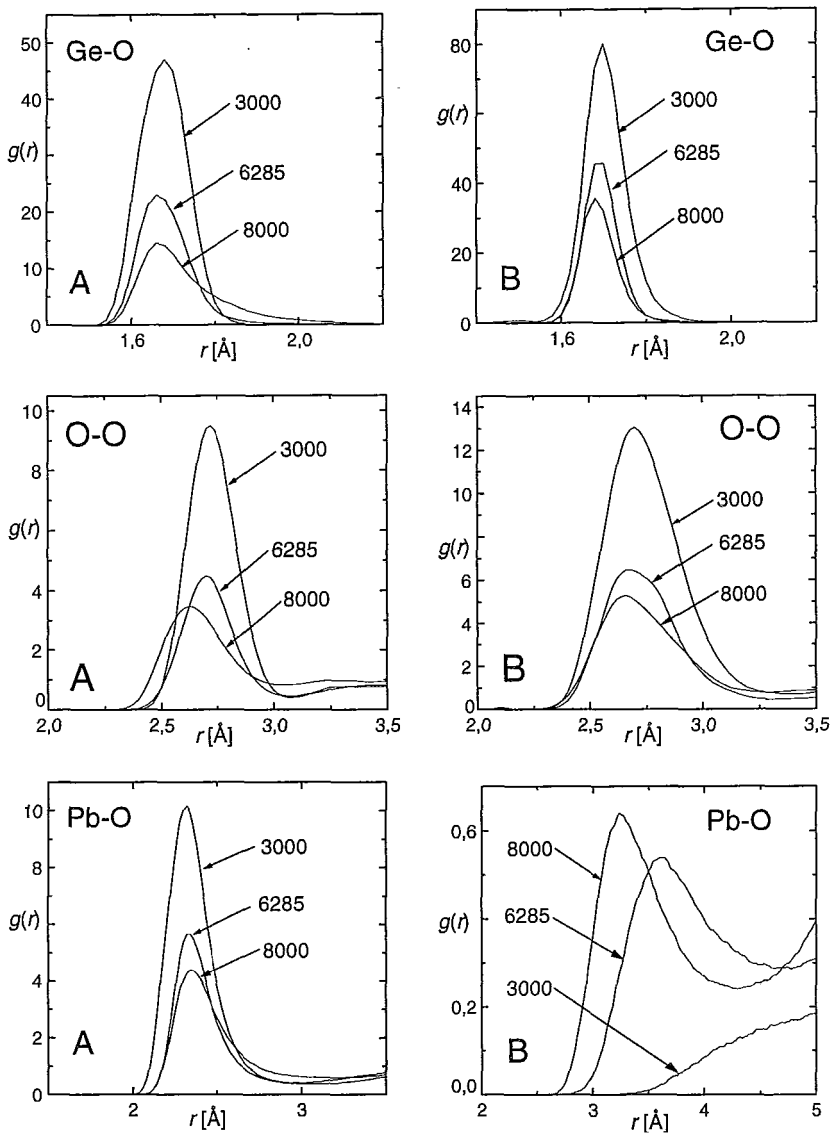

Fig. 2. Radial distribution functions related to the first co-ordination shell of Ge^{4+} and Pb^{+} cations in unreduced $PbGeO_3$ (A) and reduced $PbGeO_2$ (B) glasses. The numbers in the figures indicate the system densities in kg/m^3

Structural unit

Using the data on inter-atomic distances listed in Table I, and angle distributions from left hand side of Figure 3, one can conclude, that the GeO_4 tetrahedra are the basic structural units of the GeO_2 subsystem. They are practically the only (99.8%) structural units in the density range of 3000 ÷ 5000 kg/m^3. For 6285 kg/m^3 the fraction of tetrahedrally co-ordinated amounts to 93%,

Table I. The most probable Pb-O, Ge-O, and O-O first-neighbour distances, R_o, and the corresponding best-fit parameters R, σ^2, β and N at various densities p for the $PbGeO_3$ system

ρ [kg/m^3]	Pb-O R_o; R, σ^2, β, N	Ge-O R_o; R, σ^2, β, N	O-O R_o; R, σ^2, β, N
3000	2.32; 2.36, 0.017, 0.52, 3.54	1.68; 1.68, 0.003, 0.01. 4.02	2.72; 2.74, 0.012, 0.30, 4.04
4000	2.31; 2.36, 0.016, 0.57, 3.49	1.68; 1.68, 0.003, 0.01, 3.99	2.72; 2.74, 0.012, 0.26, 4.03
5000	2.32; 2.37, 0.016, 0.59, 3.63	1.68; 1.68, 0.003, 0.01, 4.03	2.72; 2.74, 0.011, 0.30, 4.02
6285	2.34*; (I) 2.35, 0.007, 0.40, 1.32 (II) 2.46, 0.032, 0.90, 3.00	1.67; 1.68, 0.003, 0.54, 3.99	2.70; 2.73, 0.014, 0.29, 4.1
7000	2.34*; (I) 2.33, 0.009, 0.40, 1.50 (II) 2.51, 0.033, 0.97, 3.23	1.67; 1.69, 0.004, 0.78, 4.01	2.65*; (II) 2.59, 0.010, 0.16, 0.97 (III) 2.76, 0.018, 0.69, 3.51
8000	2.34*; (I) 2.35, 0.011, 0.40, 2.09 (II) 2.58, 0.052, 0.89, 3.56	1.67; 1.72, 0.008, 1.13, 4.09	2.63*; (II) 2.59, 0.010, 0.15, 1.23 (III) 2.76, 0.033, 0.75, 4.08

R_o [Å], R [Å], σ^2 [Å^2], β - dimensionless, N - dimensionless. Asterisks indicate the R_o values for unresolved peaks

and at the density of 8000 kg/m^3 decreases down to 62%. Let us introduce the tetrahedricity parameter T_1 (after [36]), and a new, introduced herein parameter T_2:

$$T_1 = \frac{\sum_i \left(l_{O\text{-}O} - l_{O\text{-}O,i}\right)^2}{l_{O\text{-}O}^2}, \tag{4}$$

$$T_2 = \frac{\sum_i \left(l_{O\text{-}O} - l_{O\text{-}O,i}\right)^2}{l_{O\text{-}O}^2} + \frac{\sum_i \left(l_{Ge\text{-}O} - l_{Ge\text{-}O,i}\right)^2}{l_{Ge\text{-}O}^2}, \tag{5}$$

where $l_{O\text{-}O,\,i}$ and $l_{Ge\text{-}O,\,i}$ are the lengths of the i-th tetrahedrons' O-O edge (i = 1,..., 6) and Ge-O distance (i = 1,... 4), and $l_{O\text{-}O}$ and $l_{Ge\text{-}O}$ are the average O-O, and Ge-O distances, respectively. Parameters (4) and (5) are dimensionless, and being normalised to the average inter-atomic distances, characterise only the cation-O_4 groups geometry, and do not depend on particular values of bond lengths. The T_1 parameter estimates only the overall shape of the tetrahedra, with no reference to the position of central cation. The newly introduced shape estimator (5) additionally takes into account deviations in the cation localisation. The ideal tetrahedron is characterised by zero-values of both estimators, $T_1 = T_2 = 0$. The shape parameters T_1, and T_2 (and the introduced below pyramidicity parameter P, Section 4.3) refer to individual cation-O_4 groups, identified previously as local structures of tetrahedral (pyramid-like) symmetry. In particular all the cation-O_4 groups are classified at first as "pyramids" (there exists such a plane containing the cation, that all four oxygen ions lay in one of the two half-spaces determined by the plane) or "tetrahedra" (no such a plane exists). The shape-parameters calculated for all individual local structures can be of course averaged to give a single overall mean characteristic of the considered structural units. However, the normalised distributions of their values provide more information, and such distributions will be discussed below.

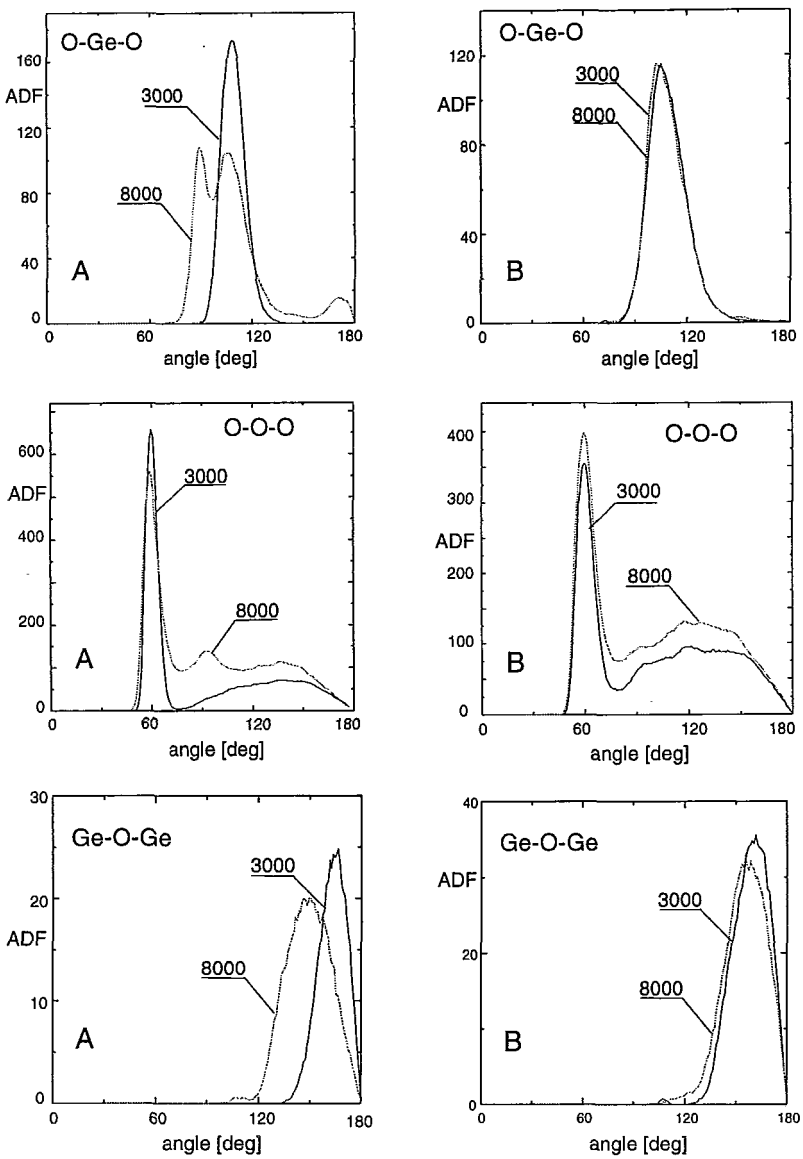

Fig. 3. O-Ge-O, O-O-O, and Ge-O-Ge angular distribution functions in unreduced $PbGeO_3$ (A) and reduced $PbGeO_2$ (B) glasses of various densities. The numbers in the figures indicate the system densities in kg/m^3

The distributions of the values of the tetrahedricity parameters T_1 and T_2 are different, although both practically do not depend on the glass density. The values of T_1 are lower than 0.02 for about 95% of all the GeO_4 units detected. The values of T_2 for each non-ideal tetrahedron are obviously higher than the corresponding values of T_1. Only 87% of the GeO_4 tetrahedra have their T_2 values lower than 0.02.

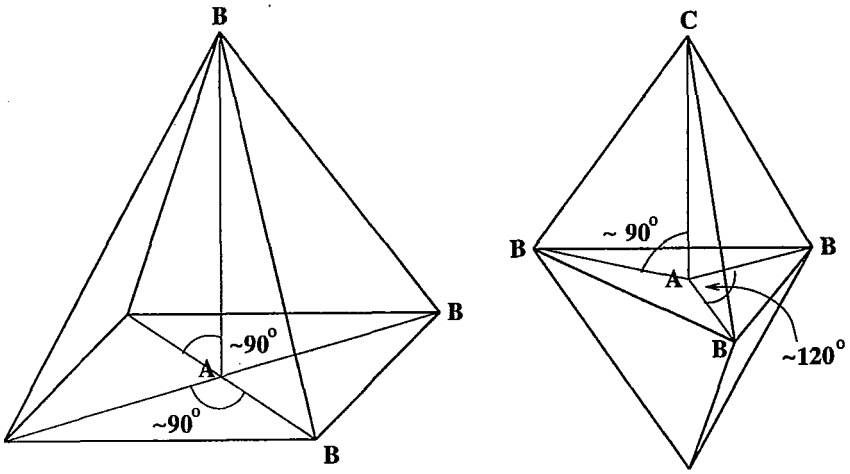

Fig. 4. Schemes of typical GeO_s and PbO_5 groups found in high-density glasses

As mentioned above, in the 6285 kg/m^3, 7000 kg/m^3, and 8000 kg/m^3 glasses 7%, 16%, and 38% of all Ge atoms, respectively, have the oxygen co-ordination different than 4. These are mainly GeO_s groups. The GeO_5 groups obtained in our simulations fall into one of two, quite well defined structures: a square pyramid, and a triangular bi-pyramid (Figure 4). The appearance of the peaks at 90° in the high-density O-O-O, and at 90° and 180° in the high-density O-Ge-O angular distributions (see Figure 3) is directly related to the geometry of the structures shown in Figure 4.

The occurrence frequency of the GeO_s groups, which all have been identified as regular square bi-pyramids, amounts to 0.4%, and 2.8% at the densities of 7000 kg/m^3, and 8000 kg/m^3, respectively. Thus, our simulations give no evidence of so called germanium anomaly (the appearance of the GeO_6 groups in the presence of other oxides in the GeO_2 glass [37-39]). This result is compatible with the recent experimental data provided by X-ray scattering analysis [40],

In the low-density structures ($\rho \leq 5000$ kg/m) cooled from the melts at higher rates ($\geq 10^{14}$ K/s), additional low peaks appear in the Ge-Ge and O-O correlations, with their maxima at about 2.92 Å, and 2.11 Å, respectively. These peaks are related to the appearance of a small number of edge-sharing GeO_4 tetrahedra. Moreover, in the rapidly cooled low-density samples, say at $\rho \leq 4000$ kg/m^3, several percent of flat GeO_3-groups have appeared [41]. No edge-sharing tetrahedra or flat GeO_3 triangles have been detected in the unreduced low-density samples being discussed herein, i.e. the ones cooled from the 10000 K-melts at the rate of $2 \cdot 10^{13}$ K/s.

4. 2. GeO_2 subsystem - reduced glasses

Table II refers to the reduced glasses, and contains the data similar to those given in Table I. Radial and angular distribution functions, related to the Ge atom neighbourhood, are shown in Figures 2 and 3 (panels B).

Table II. The most probable Ge-O, and O-O first-neighbour distances, R_o, and the corresponding best-fit parameters R, σ^2, β and N at various densities ρ for the $PbGeO_2$ system

ρ [kg/m^3]	Ge-O R_o; R, σ^2, β, N	O-O R_o; R, σ^2, β, N
3000	1.50; (I) 1.50, 0.003, 0.00, 0.03	2.11; (I) 2.11, 0.003, 0.0, 0.004
	1.70; (II) 1.71, 0.002, 0.35, 4.00	2.70*; (II) 2.63, 0.011, 0.12, 2.48
		(III) 2.85, 0.019, 0.58, 3.36
4000	1.50; (I) 1.50, 0.001, 0.00, 0.02	2.11; (I) 2.11, 0.003, 0.0, 0.004
	1.70; (II) 1.70, 0.002, 0.30, 3.87	2.70*; (II) 2.63, 0.012, 0.12, 2.29
		(III) 2.84, 0.020, 0.59, 3.53
5000	1.50; (I) 1.50, 0.002, 0.00, 0.01	2.12; (I) 2.12, 0.002, 0.0, 0.002
	1.70; (II) 1.70, 0.002, 0.33, 3.93	2.70*; (II) 2.62, 0.011, 0.11, 1.96
		(III) 2.83, 0.022, 0.59, 3.92
6285	1.50; (I) 1.51, 0.001, 0.01, 0.01	2.68*; (II) 2.60, 0.009, 0.11, 1.80
	1.70; (II) 1.70, 0.001, 0.24, 3.93	(III) 2.81, 0.019, 0.53, 4.09
7000	1.69; (II) 1.69, 0.001, 0.26, 3.94	2.68*; (II) 2.59, 0.009, 0.09, 1.72
		(III) 2.82, 0.028, 0.78, 4.91
8000	1.69; (II) 1.69, 0.002, 0.39, 3.92	2.66*; (II) 2.59, 0.012, 0.03, 1.63
		(III) 2.84, 0.041, 0.67, 5.48

R_o [Å], R [Å], σ^2 [Å^2], β - dimensionless, N - dimensionless.
Asterisks indicate the R_o values for unresolved peaks.

Inter-atomic distances

The most probable Ge-O distances, R_o, in densified reduced glasses are slightly shorter (by 0.01 Å) than those in normal- and low-density glasses, and amount to 1.69 Å, and 1.70 Å, respectively. The density dependence of the mean Ge-O distance, R, is qualitatively similar to that of R_o: the values of R decrease from 1.71 Å at 3000 kg/m^3 to 1.69 Å at 8000 kg/m^3. The values of the Debye-Waller-like parameter, σ^2, and of the skewness parameter, β, remain density-independent.

The O-O main peak can not be described by a single Γ-like function (3). However, it can be decomposed into two superimposed peaks ((II) and (III) in Table II). The σ^2 for peak (II) is stable (about 0.011 Å^2), whereas R and β slightly decrease with increasing density (Table II). The related average co-ordination number decreases from about 2.5 to about 1.6. The R parameter of peak (III) decreases from 2.85 Å at 3000 kg/m^3 to 2.81 Å at normal density and next increases to 2.84 Å at 8000 kg/m^3. It is wider and more asymmetric than peak (II). The related co-ordination numbers increase from about 3.4 for a low-density system, to about 5.5 at 8000 kg/m^3. The sub-peak identification is similar as for unreduced glasses.

In the density range from 3000 kg/m^3 to 6285 kg/m^3, very low and almost Gaussian ($\beta \approx 0.001$) peaks appear in the Ge-O and O-O correlations, with the maxima at about 1.50 Å, and 2.11 Å, respectively (peaks (I) in Table II). The average co-ordination numbers related to those pre-peaks decrease with the density increase (e.g. for Ge-O from 0.03 at 3000 kg/m^3 to 0.01 at 5000 kg/m^3), so only a very small number of close Ge-O and O-O pairs exists in the glasses. The

close Ge-O and O-O pairs are not correlated in space, and thus are not related to the same structural unit or neighbouring units. The short O-O distances appear in the edge sharing GeO_4 tetrahedra. These atom configurations give rise to the existence of several four-atom rings Ge-O-Ge-O in low-density samples of reduced glasses (see Section 5.2). On the other hand, the close Ge-O pairs have been found in triangular flat GeO_3 groups and in the most distorted GeO_4 tetrahedra. No pre-peaks in the Ge-O and O-O correlations were detected in densified systems.

Structural unit

Again, the GeO_4 tetrahedra are the basic structural units of the $Ge0_2$ subsystem. They are strongly dominating structural units in the whole density range (96-99%). The analysis of the distributions of tetrahedricity-parameters values (T_1 and T_2, equations (4), and (5), respectively) shows, that in reduced glasses the GeO_4 tetrahedra are, on the average, somewhat more distorted than in unreduced systems. Note a rather high value 5.5) of the O-O co-ordination number related to the peak (III) (Table II). This suggests that the regions rich in corner sharing GeO_4 tetrahedra appeared in the samples.

As reported in Section 4.1, a significant percentage of non-fourfold co-ordinated germanium atoms appeared only in densified $PbGeO_3$ glasses (up to 38% at $\rho = 8000$ kg/m^3). Here, in the case of $PbGeO_2$ glasses, the percentage of such germanium atoms is much lower, almost density-independent, and amounts to 1-4%. Only the GeO_3 groups (flat triangles, dominating at low densities) and the GeO_5 groups (distorted square pyramids and triangular bi-pyramids (Figure 4), dominating at high densities) were detected.

4. 3. PbO subsystem - unreduced glasses

Pb-O distances

Let us consider the first neighbours of the Pb atom in the unreduced glasses. In the considered density range the most probable Pb-O distance, R_o, slightly increases with increasing density (Table I). For rarefied glasses the Pb-O distances distribution is almost density-independent: the first RDF peak is characterised by common values of $R = 2.36$ Å, $\sigma^2 = 0.016$ Å^2, $\beta = 0.55$, and $N = 3.55$. For higher densities, however, the first Pb-O RDF's peak is poorly described by only one Γ-like function (3) (see Figure 2). The best fit parameters obtained using two functions (3) are given in Table I. It follows from the table, that the Pb ions have a two-shell neighbourhood. The first peak's medium distances, R, amount to 2.35Å, and is density independent. The second's peak medium distance increases with increasing density. For both co-ordination shells, the asymmetry degrees, β, remain density independent, whereas the Debye-Waller - like parameters, σ^2, and the co-ordination numbers increase with increasing density (Table I).

Structural unit

The O-Pb-O angular distribution functions for several densities are shown in Figure 5. The presence of the 60°-, and 90°-angles is readily seen. The decomposition of the humps in the wide

angles region into several Gaussian peaks suggests the elevated appearance of the 109°-, 120°-, 145°-, and 170°-angles. The occurrence ratios of various angles are strongly density-dependent. This suggests that the Pb atoms have a number of various neighbourhoods.

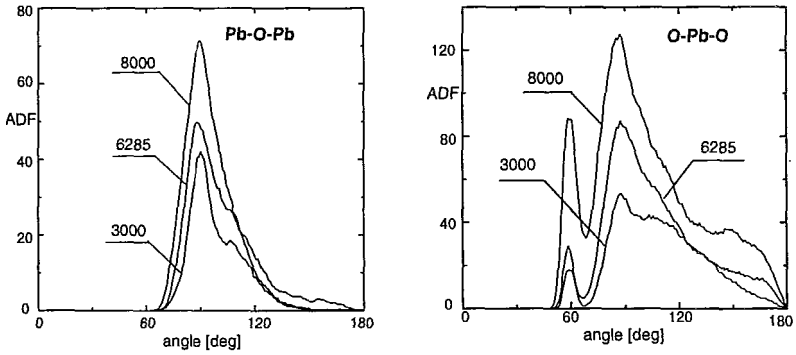

Fig. 5. O-Pb-O and Pb-O-Pb angular distribution functions in $PbGeO_3$ glasses of various densities

The fraction of lead atoms co-ordinated with four oxygen atoms depends on the system density: in the range 3000-5000 kg/m^3 it increases from 55% to 65% (the maximum value), and for 6285 kg/m^3, 7000 kg/m^3 and 8000 kg/m^3 amounts to 47%, 24% and 4%, respectively. The PbO_4 groups were identified as regular tetrahedra (90-95%) or square pyramids (10-50%). The values of the tetrahedricity parameters T_1 and T_2 for PbO_4 tetrahedra are higher than for GeO_4 ones. No clear dependence of the T_1 or T_2 values distribution on the density could be found. The T_2 values are on average higher than the corresponding T_1 values by about 10% only. In all the densities, T_1 is lower than 0.2 for about 90% of all PbO_4 tetrahedra, i.e. the PbO_4 tetrahedra are much less regular than the $Ge0_4$ ones. Note, that for the glasses cooled at higher rate [41], the percentage of PbO_4 groups was significantly lower (by 10-20%), and only 60-80% of these groups had tetrahedral symmetry. This fact allows one to expect that at lower cooling rates than reported in the present paper, the PbO_4 groups would have almost entirely tetrahedral structure, with quite marginal admixture of pyramidal units. Indeed, the square-pyramidal PbO_4 units detected in our simulations are very irregular. The latter statement results from inspection of the distributions of shape estimator, P, defined as:

$$P = \frac{\sum_i \left(l_{\text{Pb-O}} - l_{\text{Pb-O},i}\right)^2}{l_{\text{Pb-O}}^2} + \frac{\sum_i \left(l_{\text{O-O}} - l_{\text{O-O},i}\right)^2}{l_{\text{O-O}}^2}, \tag{6}$$

where $l_{\text{Pb-O},\,i}$ is the length of the i-th Pb-O edge, and $l_{\text{Pb-O}}$ is the average length of the Pb-O edges, and similarly, $l_{\text{O-O},\,i}$ is the length of the i-th O-O edge, and $l_{\text{O-O}}$ is the average length of the O-O edges. The distributions of P values for pyramid-like PbO_4-groups do not show any correlation with the system density, and are rather widely distributed. We think that the poor statistics for P can not be attributed only to relatively small number of detected pyramids. In our opinion, the detected PbO_4 pyramids are rather accidental metastable frozen-in defects, related to not sufficiently slow cooling rate applied in our simulations, than true structural units of the $PbGeO_3$ glass.

As stated above, only certain fractions of all Pb atoms have four-fold oxygen co-ordination. Let us describe in brief other types of lead atom neighbourhoods.

In the low-density range ($\rho \leq 5000$ kg/m^3) about 30% of lead atoms has 3-fold oxygen co-ordination, and form roughly triangular pyramids. A small fraction (1-2%) of lead atoms with two oxygen neighbours was found. About 10% of Pb atoms have five-fold co-ordination. Among these neighbourhoods distorted square pyramids and triangular bi-pyramids (Figure 4) were detected. Several PbO_5 groups could not be classified.

At normal density there are about 40% of Pb atoms have the 5-fold co-ordination, mostly of bi-pyramid-like symmetry. 10% of lead atoms has six oxygen neighbours.

In the high-density unreduced glasses there are no PbO_3 groups, and most of the Pb atoms have more than four oxygen-neighbours. The 5-, 6- and 7-atom shells appear for 53%, 19%, and 4% of Pb atoms, and for 34%, 47%, and 15% of Pb atoms in the 7000 kg/m^3 and 8000 kg/m^3 glasses, respectively. All these high-density structural units, particularly with 6- and 7-fold co-ordination, show poor symmetry, and can not be unambiguously classified.

5. MEDIUM-RANGE ORDER

As far as the short-range order is concerned, the inspection of the radial and angular distribution functions permits a rather detailed description of the first co-ordination shells of the atoms. In order to describe the second and further co-ordination shells, i.e. to describe the medium-range order, despite of analysing the RDFs and ADFs (Section 5.1) we use the cation-anion ring analysis (Sections 5.2 and 5.3).

5.1. The Ge-Ge, Pb-Ge, and Pb-Pb radial correlations

In Figure 6, the first RDFs' peaks for Ge-Ge, Pb-Ge and Pb-Pb pairs in the $PbGeO_3$ (panels A), and $PbGeO_2$ (panels B) systems are shown. The peak profile parameters are listed in Tables III and IV. Examples of cation-cation-cation angular correlations in the $PbGeO_3$ glasses of various densities are presented in Figure 7.

Ge-Ge correlations

One can easily note a relative stability of the inter-atomic Ge-Ge distances in both unreduced, and reduced glasses. In the $PbGeO_3$ system a distinct change of the first co-ordination number occurs: from about two for 3000 kg/m^3 to about three for 8000 kg/m^3. The range of variability of the Ge-Ge co-ordination in the $PbGeO_2$ system is much smaller (3.9 - 4.2 between the limiting densities). In both unreduced and reduced glasses, the Ge-Ge distance closes a triangle, in which two edges have the Ge-O distance length, and the Ge-O-Ge angles equal to the peak positions of the lower panels of Figure 3. Thus, the first Ge-Ge peak corresponds to corner-sharing GeO_4 tetrahedra. The Ge-Ge co-ordination number close to 4 in reduced glasses means, that most of germania is structured similarly as pure amorphous GeO_2, and thus must be concentrated in volumes privy of the Pb atoms.

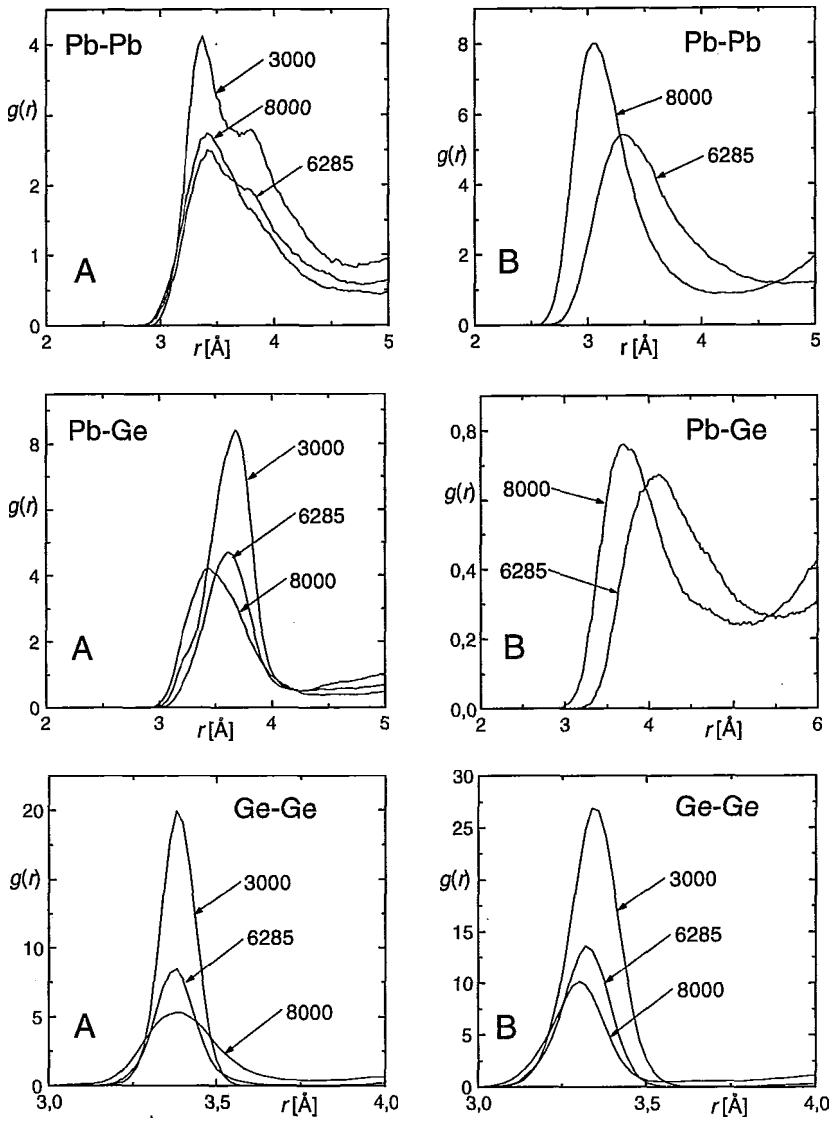

Fig. 6. Cation-cation radial distribution functions in unreduced $PbGeO_3$ (A) and reduced $PbGeO_2$ (B) glasses

The wide irregular humps in the Ge-Ge-Ge angular correlations, both in unreduced and reduced glasses, are difficult to interpret. However, there are no doubts that the distributions are peaked at about 60°, 90° and 110°.

Pb-Pb correlations

In unreduced glasses, $PbGeO_3$, the first Pb-Pb peak splits into two sub-peaks. The first sub-peak is rather narrow, and has its R values remain in the range from 3.38 Å to 3.40 Å. The second sub-peak is significantly wider, and its R moves from about 3.90 Å in the low density limit to

about 4.1 Å in the high density limit. The interpretation of these two sub-peaks will be given in Section 5.3. The co-ordination numbers associated with the sub-peaks increase from about 1.1, to about 2.1 for the first peak, and from about 1.7, to about 3.8 for the second peak. This corresponds to the increase (with increasing density) of the total average co-ordination number related to the first double co-ordination shell roughly from three to six.

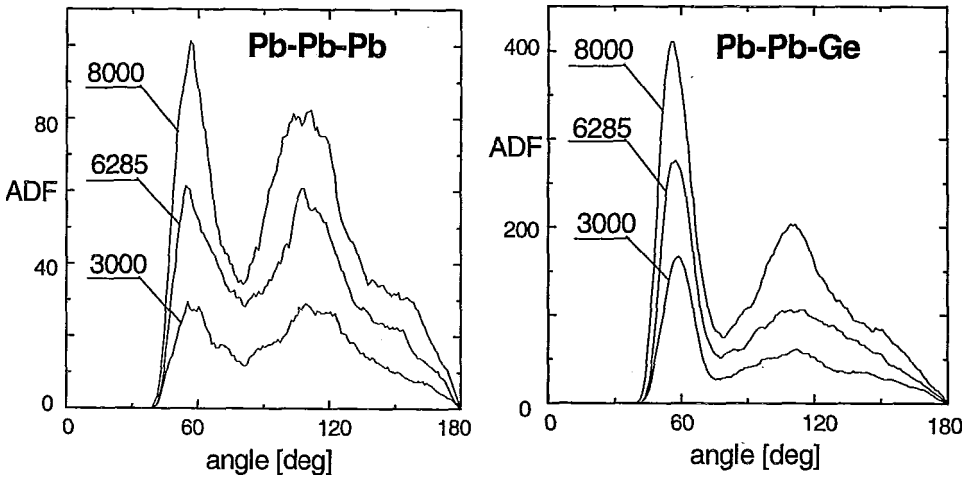

Fig. 7. Pb-Pb-Pb and Pb-Pb-Ge angular distribution functions in $PbGeO_3$ glasses of various densities

Table III. The most probable distances, R_o, and the best fit R, σ^2, β, N parameters for the Pb-Pb, Pb-Ge, and Ge-Ge correlations at various densities ρ for the $PbGeO_3$ system

ρ [kg/m^3]	Pb-Pb R_o; R, σ^2, β, N	Pb-Ge R_o; R, σ^2, β, N	Ge-Ge R_o; R, σ^2, β, N
3000	3.38*; (I) 3.39, 0.018, 0.25, 1.11 (II) 3.90, 0.062, 0.35, 1.67	3.68*; (I) 3.29, 0.015, 0.27, 0.28 (II) 3.67, 0.029, 0.02, 3.29	3.39; 3.39, 0.003, 0.02, 2.08
4000	3.38*; (I) 3.39, 0.020, 0.21, 1.02 (II) 3.97, 0.120, 0.52, 1.95	3.68*; (I) 3.32, 0.018, 0.01, 0.32 (II) 3.69, 0.024, 0.01, 3.24	3.39; 3.39, 0.003, 0.0, 2.04
5000	3.38*; (I) 3.38, 0.022, 0.24, 1.00 (II) 3.98, 0.124, 0.65, 2.60	3.69*; (II) 3.45, 0.040, 0.69, 0.70 (III) 3.71, 0.022, 0.03, 2.91	3.40; 3.39, 0.003, 0.01, 2.08
6285	3.42*; (I) 3.38, 0.027, 0.16, 1.41 (II) 3.98, 0.122, 0.84, 3.02	3.62*; (II) 3.49, 0.034, 0.40, 1.46 (III) 3.70, 0.030, 0.35, 3.00	3.38; 3.38, 0.004, 0.07, 2.12
7000	3.44*; (I) 3.40, 0.028, 0.19, 1.71 (II) 4.04, 0.171, 0.16, 3.48	3.59*; (II) 3.44, 0.025, 0.18, 2.02 (III) 3.74, 0.032, 0.48, 3.09	3.37; 3.38, 0.005, 0.24, 2.33
8000	3.42*; (I) 3.40, 0.038, 0.25, 2.13 (II) 4.07, 0.200, 0.98, 3.80	3.44*; (II) 3.48, 0.055, 0.76, 3.36 (III) 3.74, 0.080, 0.73, 3.01	3.38; 3.40, 0.011, 0.30, 2.99

R_o [Å], R [Å], σ^2 [Å^2], β - dimensionless, N - dimensionless. Asterisks indicate the R_o values for unresolved peaks.

Table IV. The most probable distances, R_o, and the best fit R, σ^2, β, N parameters for the Ge-Ge correlations at various densities p for the $PbGeO_2$ system

ρ [kg/m^3]	Ge-Ge R_o; R, σ^2, β, N
3000	3.35; 3.35, 0.005, 0.02, 3.89
4000	3.34; 3.34, 0.004, 0.01, 3.87
5000	3.34; 3.34, 0.005, 0.07, 3.95
6285	3.32; 3.33, 0.005, 0.03, 3.97
7000	3.32; 3.32, 0.005, 0.01, 4.07
8000	3.32; 3.32, 0.006, 0.02, 4.19

R_o [Å], R [Å], σ^2 [Å^2], β - dimensionless,
N - dimensionless

The spatial distribution of the lead atoms in reduced glasses, $PbGeO_2$, is quite different. As results from the shape of the Pb-O (Figure 2), Pb-Ge and Pb-Pb (Figure 6) RDFs, and the corresponding co-ordination numbers, in reduced glasses a strong non-uniformity in the lead atoms occurs. On reduction, the average Pb-Pb co-ordination increases significantly: from about 4 to about 10 at ρ = 6285 kg/m^3, and from about 6 to almost 11 at ρ = 8000 kg/m^3. Simultaneously, the Pb-O and Pb-Ge co-ordination numbers decrease: from 4.5 to 2.5, and from 4 to 2.5, respectively, at normal density, and from 5.5 to 2.5 and from 6.4 to 2.5, respectively, at ρ = 8000 kg/m^3. This means, that in the reduced system only a small fraction of Pb atoms has oxygen atoms as their first neighbours (and germanium atoms as the second neighbours), and most of the Pb atoms are highly co-ordinated by Pb atoms. This effect is readily seen on direct visualisation of the atom distribution (Figure 8), The Voronoï analysis fully supports the conclusions drawn from the inspection of the radial distribution functions and the co-ordination numbers. In particular, in the reduced normal-density sample 97.2% of lead atoms belongs to one cluster of face sharing Pb Voronoï polyhedra. Out of the remaining 2.8% of the Pb atoms, 2.4% of them is contained in isolated polyhedra, and 0.4% belongs to two-element clusters. About 40% of the Pb atoms have the Pb-Pb co-ordination not lower than twelve, and almost 90% have at least six Pb atoms in their first co-ordination shells. The latter two parameters are somewhat higher for the 7000 kg/m^3 and 8000 kg/m^3 glasses (by several percent). Thus, the aggregation tendency in densified reduced glasses is not worse than at the normal-density phase (although the high-temperature diffusion coefficient of Pb atoms is at 8000 kg/m^3 about two times smaller than at 6285 kg/m^3). The structure of the bulk parts of the resulting lead granules is in one-third of the *hcp* type, in one-third of the *fcc* type, and in one-third - amorphous. Thus, the metal granules obtained in our simulations do not have the correct *fcc* structure. This fact is due to the over-simplified form of our Pb-Pb interaction (only repulsive terms of exponential dependence on ***r***). For this reason we do not discuss the granule formation in the low-density samples, where the attractive parts of interactions must not be neglected on any modelling level.

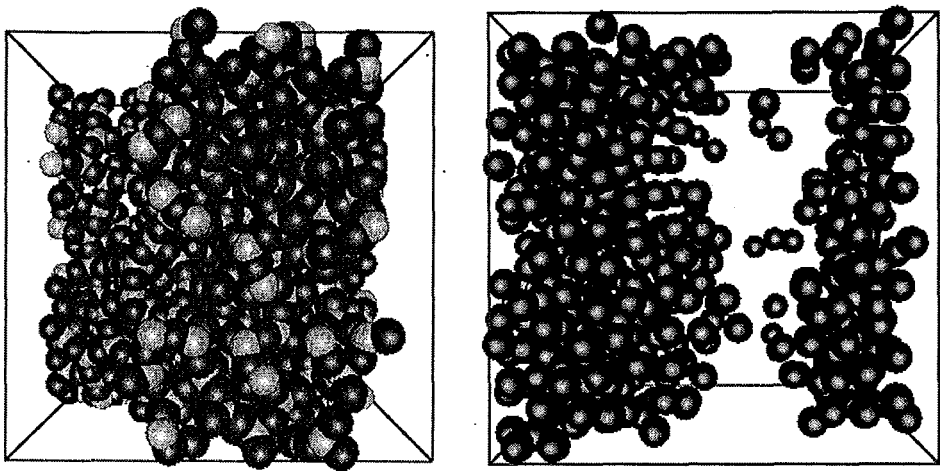

Fig. 8. The snapshots of the atom configurations in the last simulation step for the normal-density $PbGeO_2$. Left panel - Ge (azure) and O (red) atoms only, right panel - Pb atoms only. The simulation box contain 2000 atoms

Pb-Ge correlations

The first Pb-Ge peak in unreduced glasses is also composed, and in general splits into three sub-peaks. The shortest correlation, with the *R*-value of about 3.3 Å, is present in low-density samples, ($\rho \leq 4000$ kg/m^2). Since the related average co-ordination number is very low, only few Pb-Ge pairs contribute to this peak. The second peak (II) has its *R*-values in the range from 3.45 Å to 3.48 Å, and the third (III) peak in the range from 3.71 Å to 3.74 Å, in both cases showing the tendency to increases with increasing density. The co-ordination numbers associated with the (II) sub-peak increase from less than one, to over three. The co-ordination number associated with sub-peak (III) does not vary too much with the glass density, and amounts to about three. This corresponds to the increase (with increasing density) of the total co-ordination number related to the unresolved first RDF's peak roughly from 3.6 to 6.4.

5. 2. Ge-O-Ge-O-... rings in unreduced and reduced glasses

A closed chain of chemically bonded atoms, consisting of *N* cations and *N* anions is called an *N*-member ring. In what follows we discuss the length statistics of linearly independent (basal) rings that span the full graph representing chemically bonded atoms. 2-member rings correspond to edge-sharing or face-sharing structural units. Since in most of "well relaxed" structural models of SiO_2 and GeO_2 the rings of lengths equal to 5, 6, and 7 dominate, the 3-, and 4-member rings are usually referred to as "strained" rings [42,43].

The connectivity graphs for Ge and O ions were calculated using an adjacency criterion with cut-off radii equal to 2.1 Å. Figure 9 shows the length distribution of the Ge-O-Ge-O-... rings for all the considered densities.

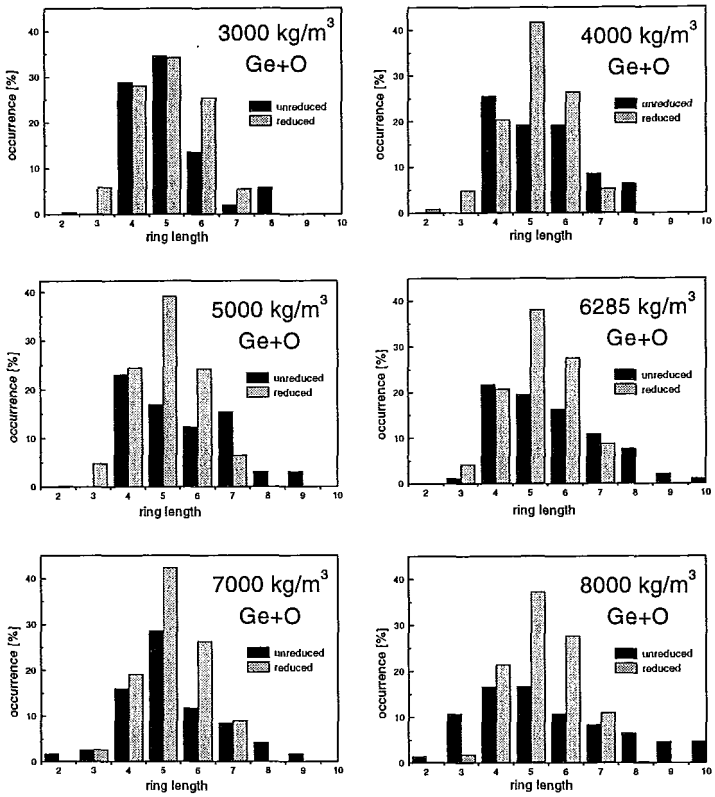

Fig. 9. Comparison of distributions of the Ge-O-Ge-O-... rings' lengths in unreduced and reduced glasses of various densities

The fraction of 2-member rings, corresponding to edge sharing GeO_4 tetrahedra, is marginal for all the densities. The origin of the low-density 2-member rings in reduced glasses has been explained in Section 4.2. In the high-density 2-member rings in unreduced glasses the diagonal O-O distance fall into the left wing of the main spatial correlation, and thus no associated pre-peak could be observed.

The density-dependence of the percentage of 3-member rings is quite different in unreduced and reduced glasses. In the former case, the fraction of 3-member rings is negligible in the low-density samples, and significantly increases in the high-density samples. On the other hand, in the reduced glasses, a certain (almost density independent) fraction of 3-member rings exist in the rarefied samples. Their contributions becomes smaller in high-density samples.

The fraction of 4-member rings in the $PbGeO_3$ system decreases from about 30% to about 20% in the density range from 3000 kg/m^3 up to the normal density, and amounts to about 15% in densified glasses. The fraction of 4-member rings in the $PbGeO_2$ system is the highest at 3000 kg/m^3 (about 30%), and from 4000 kg/m^3 on remains roughly density independent (a 20% contribution).

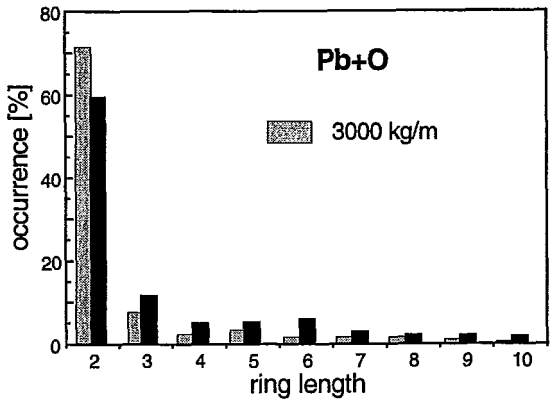

Fig. 10. Distributions of the Pb-O-Pb-O-... rings' lengths in the $PbGeO_3$ glasses of various densities.

The density-dependence of the fraction of exactly 5-member rings in unreduced glasses is less regular. However, looking at the density dependence of the rings' length distribution for rings longer than four one notes an evident tendency. From $\rho = 5000$ kg/m^3 on, with increasing density longer and longer rings appear. At the normal density single rings of length up to 20 were detected. Simultaneously, at low densities practically no long (longer than 8 in our case) rings are present. In the reduced glasses, the 5-member rings are the most frequent for all the densities. Moreover, in the whole density range no rings longer than 7 have been detected.

5. 3. Pb-O-Pb-O-... rings in unreduced glasses

The connectivity graphs for Pb and O ions in $PbGeO_3$ were calculated using an adjacency criterion with cut-off radii equal to 3.0 Å.

In Figure 10, the lead-oxygen rings' distributions at 3000 kg/m^3 and 8000 kg/m^3 are compared with the corresponding distribution for the normal density. As it is seen, with decreasing density, the lead-oxygen basal rings become systematically shorter: the rings of the lengths higher than 3 are less frequent, and the contribution of the 2-member rings (corresponding to edge sharing lead-related structural units) increases. Such an evolution of the Pb^{2+}-O^{2-} rings' lengths suggests, that with the density decrease, the structural units related to lead cations tend to form more and more compact groups, inter-connected with the Pb-O-Pb-O-... or GeO_4-Pb-GeO_4-Pb-GeO_4-... chains.

The Pb-O-Pb and O-Pb-O angles' distributions along the 2-member rings have been calculated. The distributions only weakly depend on the system density, and in general become somewhat wider with increasing density. For all the densities over 50% of all values of the Pb-O-Pb angles fall into the interval from 80° to 90°, and the distribution tails have only a 10°-width. As far as the O-Pb-O angles are concerned, for $\rho \leq 6285$ kg/m^3 also 50% of the angles falls into the same range from 80° to 90°, with similar widths of the distribution tails. However, in densified glasses the occurrence maximum of the O-Pb-O angles shifts to lower angles, and 45% of the angles enter the interval from 70° to 80°. Thus, the shape of the 2-member lead-oxygen rings does not depend very much on the system density, and the Pb-O-Pb angles are stiffer than the O-Pb-O angles. The angular distributions along the 2-member rings described above are to

be compared with corresponding distributions averaged over the whole simulation box, Figure 5. The main peaks in this Figure are related predominantly to the 2-member rings, whereas other peaks and humps correspond to the O-Pb-O and Pb-O-Pb angles, in which the oxygen and lead atoms belong to adjacent (vertex- or side-sharing) rings.

In Section 5.1 the complex structure of the first Pb-Pb RDF has been described. From the analysis of the lead-oxygen rings' geometry it results, that the shorter Pb-Pb distances (peak (I)) originates from the diagonal distances within the 2-member Pb-O rings. The corresponding O-O diagonal distances contribute to wide RDFs' features between 3.3 Å and 3.6 Å, absent in the reduced glasses, where there are no P b - O rings (see Figure 2).

6. CONCLUSIONS

We have presented the results of extensive MD simulations of unreduced PbGeOj and reduced $PbGe0_2$ glasses in the density range from 3000 kg/m^3 to 8000 kg/m^3. As mentioned in Section 2, for $p \leq 6285$ kg/m^3, the obtained glasses are stable (maintain their densities during the zero external pressure simulations), whereas the densified glasses expand continuously during the volume relaxation runs, so the results correspond to non-equilibrium pressure-induced structures.

The analysis of our MD-simulation data suggests the following conclusions:

1) the short range ordering around germanium atoms changes rather slightly in the density range 3000-8000 kg/m^3. Both for unreduced, and reduced glasses, regular GeO_4 units dominate in the GeO_2 subsystem for all the densities. No germanium anomaly is reported.
2) The PbO subsystem in unreduced glasses has much more complex structure. Among the PbO_4 structural units (identification cut-off radius of 3.0 Å) both regular tetrahedra and regular square pyramids were detected. With increasing density the contribution of 4-co-ordinated lead ions decreases, and the fraction of lead atoms with five-, six-fold oxygen co-ordination becomes significant. The PbO_5 groups appear in two rather well defined forms: square pyramids with the oxygen atoms in the corners and the Pb atom in the centre of the oxygen basal square (or slightly over this point), and triangular bi-pyramids (Figure 4). The PbO_6 and PbO_7 groups show poor symmetry and could not be classified.
3) The medium range order undergoes changes, qualitatively different in unreduced, and reduced glasses. Both in unreduced and reduced glasses, the 4-, 5- and 6-member Ge-O rings dominate. In the former case, on increasing density the number of shorter, strained rings significantly increases. In highly rarefied unreduced glasses, in contrast to the normal- and high-density phases, the Ge-O rings longer than 8 are absent. The distributions of the Ge-O rings' lengths in reduced glasses are always narrower than in the unreduced ones and the 5-member rings are the most frequent for all the densities. In contrast to the unreduced glasses no rings longer than seven have been detected, and short rings appear at low densities rather than at high densities. Note that the ring analysis provides much more information (also quantitative) than the study of second-neighbour spatial correlations (radial and angular). However, the geometric interpretation of longer

rings is still difficult, mainly because of their small populations and thus poor statistics. In order to classify rings longer than 3 much larger samples are needed.

4) In the $PbGeO_2$ glasses an evident phase separation occurs. The atoms, initially uniformly distributed within the simulation box, during cooling arrange themselves to form pure GeO_2 glass and Pb phases.

Acknowledgement

The opportunity to perform our simulations at the TASK Computer Centre in Gdansk is kindly acknowledged.

The work has been partially supported by KBN, grant 7 T08D 009 20.

References

[1] Ruller J. A., Shelby J. E„ Phys. Chem. Glass., **33**, 177 (1992).
[2] Dumbaugh W„ Lapp J. C., J. Am. Ceram. Soc., **75**, 2315 (1992).
[3] Yamada K., Matsumoto A., NiimuraN., Fukunaga T., Hayashi N., Watanabe N., J. Phys. Soc. Jap., **55**, 831 (1986).
[4] Cormier G., Peres T., Capobianco J. A., J. Non-Cryst. Sol., **195**, 125 (1996).
[5] Feltz A., *Amorphous Inorganic Materials and Glasses,* VCH, Weinheim 1993.
[6] Lezal D„ Pedlikova J. I., Hovak J., J. Non-Cryst Sol, **196**,178 (1996).
[7] Rajiv W. J., Kalia K„ Vashishta P, Rino J. P., Phys. Rev., **B50**, 118 (1994).
[8] Olivi-Tran N„ Jullien R„ Phys. Rev., **B52**, 258 (1995).
[9] Valle R. G. D„ Venuti E, Phys. Rev., **B54**, 3809 (1996).
[10] Rat E, Foret M, Courtens E, Vacher R, Arai M, Phys. Rev. Lett, **83**, 1355 (1999).
[11] Vacher R, Courtens E, Foret M, Hehlen B, Rat E, Casalta H, Dorner B, Physica, **B276-278**, 427 (2000).
[12] Ishikawa K, Uchiyama Y„ Ogawa H, Fujimura S, Appl. Surf. Sci, **117-118**, 212 (1997).
[13] Zhu D. M, Weng H. F, J. Non-Cryst. Sol, **185**, 262 (1995).
[14] Woignier T„ Duffours L„ Phalippou J, J. Non-Cryst. Sol, **194**, 283 (1996).
[15] Hiramatsu A, Arai M, Shibazaki H, Tsunekawa M, Otomo T, Hannon A. C, Bennington S. M, Physica, **B219-220**, 287 (1996).
[16] Vogel E. M„ Grabow M. H, Martin S. W, J. Non-Cryst. Sol, **204**, 95 (1996).
[17] Tan C. Z„ Arndt J, Xie H. S, Physica, **B252**, 28 (1998).
[18] Tan C. Z„ Arndt J, J. Non-Cryst Sol, **249**, 47 (1999).
[19] Inamura Y, Arai M, Nakamura M, Otomo T, Kitamura N, Bennington S. M, Hannon A. C, J. Non-Cryst. Sol, (2000) in print.
[20] Hannon A. C, 2000 - private communication.
[21] Rybicka A, *The structure and properties of lead-silicate and lead-germanate glasses: a molecular dynamics study,* PhD thesis, Technical University of Gdansk, Gdansk 1999.
[22] Brostow W, Chybicki M, Laskowski R, Rybicki J, Phys. Rev, **B57**, 13448 (1998).
[23] Laskowski R„ Rybicki J, Chybicki M, TASK Quart, **1**, 96 (1997).
[24] Laskowski R, TASK Quart, **4**, 531 (2000).
[25] Rybicki J, Laskowski R, Feliziani S, Comp. Phys. Commun, **97** 185 (1996).
[26] Balducci R„ Pearlman R. S„ J. Chem. Inf. Comput. Sci, **34**, 822 (1994).
[27] Mancini G, TASK Quart, **1**, 89 (1997).
[28] Mancini G, Comp. Phys. Commun. (2000) submitted.

[29] Bergmański G., Rybicki J., Mancini G., TASK Quart., **4**, 555 (2000).
[30] Rybicki J., Bergmanski G., Mancini G., J. Non-Cryst. Sol., (2000) submitted.
[31] Mazurin O. W., Strielcina M. W., Szwajko-Szwajkowskaja T. P., *Svoistva stiekol i stieklo-obrazuiuszczich rasplavov,* vol. II, Nauka, Leningrad 1982.
[32] Mazurin O. W., Strielcina M. W., Szwajko-Szwajkowskaja T. P., *Svoistva stiekol i stieklo-obrazuiuszczich rasplavov,* vol. V, Nauka, Leningrad 1987.
[33] Filipponi A., J. Phys. CM, **6**, 8415 (1994).
[34] D'Angelo P., Di Nola A., Filipponi A., Pavel N. V., Roccatano D., J. Chem. Phys., **100**, 985 (1994).
[35] Filipponi A., Di Cicco A., Phys. Rev., **B51**,12322 (1995).
[36] Medvedev N. N., Naberukhin Y. I., J. Non-Cryst. Sol., **94**, 402 (1987).
[37] Ribeiro S. L., Dexpert-Ghys J., Piriou B., Mastelaro V. R., J. Non-Cryst. Sol., **159**, 213 (1993).
[38] Ruller J. A., Shaw C. M., Shelby J. E., Phys. Chem. Glass., **33**, 161 (1992).
[39] Umesaki N., Brunier T. M., Wright A. C., Hannon A. C., Sinclair R. N., Physica, **B213-214**, 490 (1995).
[40] Červinka L., J. Non-Cryst. Sol., (2000) in print.
[41] Rybicki J., Witkowska A., Bosko J., Mancini G., Feliziani S., Opt. Appl., **30**, 701 (2000).
[42] King S. V., Nature, **213**, 1112 (1967).
[43] Hamann D. R., Phys. Rev., **B55**, 14784 (1997).